Relation between crystal structure and optical properties in the correlated blue pigment $YIn_{1-x}Mn_xO_3$

Valentin Ransmayr,[1] Jan M. Tomczak,[1] and Anna Galler[1,2]
[1]*Institute of Solid State Physics, TU Wien, 1040 Vienna, Austria*
[2]*Max Planck Institute for the Structure and Dynamics of Matter, 22761 Hamburg, Germany*

(Received 8 August 2022; accepted 12 October 2022; published 28 October 2022)

A material's properties and functionalities are determined by its chemical constituents and the atomic arrangement in which they crystallize. For the recently discovered pigment $YIn_{1-x}Mn_xO_3$, for instance, it had been surmised that its bright blue color owes to an unusual, trigonal bipyramidal, oxygen coordination of the manganese impurities. Here, we demonstrate that, indeed, a direct correspondence between details of the local Mn environment and the pigment's blue color holds: Combining realistic many-body calculations (dynamical mean-field theory to treat the quasi-atomic Mn-multiplets at low doping $x = 8\%$) with an effective medium description (Kubelka-Munk model to describe scattering in a milled pigment sample), we find that only a Mn-coordination polyhedra consisting of two distorted oxygen pyramids results in a diffuse reflectance commensurate with the experimental blue color. We motivate that the distortion of the bipyramid helps circumventing atomic selection rules, allowing for dipolar d-d transitions and creating the desired two-peak absorption profile.

DOI: 10.1103/PhysRevMaterials.6.105003

I. INTRODUCTION

While some famous blue pigments—among them ultramarin blue (lapis lazuli), Han blue, and Egyptian blue—have been known since antiquity, most synthetic blue pigment materials were discovered with the advent of modern chemistry. Some of them, such as cobalt blue $CoAl_2O_4$, Prussian blue $Fe_4(Fe[CN]_6)_3$, and azurite $Cu_3(CO_3)_2(OH)_2$ [1], however, suffer from environmental or durability issues, such that the search for new earth-abundant and environmentally-benign alternatives has remained an active field of research. Thus, it was good news when a new, stable inorganic blue pigment material, $YIn_{1-x}Mn_xO_3$, was synthesized at Oregon State University in 2009 [2]. Discovered by serendipity, this novel blue pigment [3] turned out to be ideal for many potential applications from ceramic glazes [4–6] and industrial coatings to plastics and artists' paint [7]. It is being industrially produced under the name YInMn blue since 2017 [7,8].

$YInO_3$ and $YMnO_3$ are commonly known in the perovskite structure [10], but they can also be prepared in the hexagonal $P6_3cm$ structure [11] shown in Fig. 1: It consists of layers of corner-sharing, slightly tilted MO_5 (M = In, Mn) trigonal bipyramids (TBP), separated by layers of Y^{3+} ions. The researchers at Oregon State University were interested in potential multiferroic properties of hexagonal YMO_3, when they noticed that replacing some In by Mn was inducing a brilliant blue color over a wide range of the paramagnetic $YIn_{1-x}Mn_xO_3$ (with $x = 0.02 - 0.2$) solid solution [2,3]. This finding was all the more surprising since pure $YInO_3$ and $YMnO_3$ are white and black, respectively. From further experimental investigations of the materials' crystal and electronic structure, it was concluded that the blue color of $YIn_{1-x}Mn_xO_3$ must be a consequence of the unusual TBP coordination of the Mn^{3+} ions, which determines the crystal-field splitting of the Mn $3d$ shell [2]. A special role was attributed to the axial Mn-O bond distances, which are considerably shorter than the axial In-O bonds in $YInO_3$ [2,12]. Indeed, further investigations [13,14] underlined the importance of the local crystalline environment around the Mn^{3+} ions for the color of the pigment. In Ref. [14], x-ray absorption near edge structure (XANES) and extended x-ray absorption fine structure (EXAFS) spectroscopy investigations revealed the presence of two different TBP environments in $YIn_{1-x}Mn_xO_3$: one with symmetric and another one with asymmetric axial Mn-O bonds in the MnO_5 bipyramids. The distorted TBP, with asymmetric axial Mn-O bonds, was found to be dominant in the regime of low Mn concentrations x and claimed to be responsible for the blue coloration. The experimental findings in Refs. [2,14] were supported by structural relaxations within density functional theory (LSDA+U) simulations. However, no explicit calculation of the electronic structure and the optical response of $YIn_{1-x}Mn_xO_3$, which could provide a direct link between structural information and the optical transitions responsible for the blue color, has been presented yet.

Indeed, systems like $YIn_{1-x}Mn_xO_3$ represent a challenge for modern electronic structure theory: First, a description of the Mn dopant and the correlation effects hosted by its open $3d$ shell requires many-body methods beyond standard density functional theory (DFT-LDA). Second, the need for

Published by the American Physical Society under the terms of the Creative Commons Attribution 4.0 International license. Further distribution of this work must maintain attribution to the author(s) and the published article's title, journal citation, and DOI. Open access publication funded by the Max Planck Society.

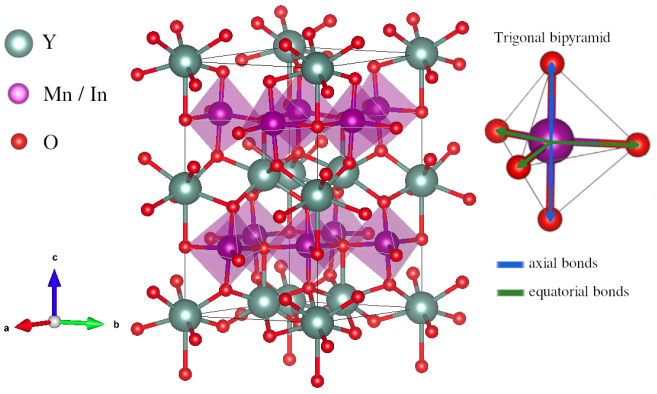

FIG. 1. Crystal structure of YMO_3 (with M = Mn, In: purple spheres, O: red spheres, Y: green spheres). The structure consists of layers of corner sharing, slightly tilted MO_5 trigonal bipyramids (TBP), separated by Y buffers. The inset on the right depicts a MO_5 TBP with equatorial and axial M-O bonds (visualization with VESTA [9]).

accurate optical gaps also calls for an advanced treatment of ligand states beyond simple DFT functionals. Therefore, only few theoretical studies regarding the color of correlated pigment materials are available to date [15–17]. Blue pigments are particularly difficult to simulate, since they require a two-peak structure in the optical absorption, which ensures that only blue light is reflected, while all other colors are absorbed. Red or yellow pigments, instead, are conceptually easier since they only require the absorption edge (hence the optical gap) to be at the right position.

In this paper, we employ the recently developed mBJ@DFT+DMFT approach [16,18,19] to compute the electronic structure and optical conductivity of $YIn_{1-x}Mn_xO_3$. We focus on a Mn concentration of $x = 8\%$, for which a brilliant blue color is observed in experiment. The methodology combines an improved description of nonlocal exchange-driven band-gaps via the semilocal modified Becke-Johnson (mBJ) [20,21] potential with an advanced treatment of the strongly correlated Mn $3d$ states within dynamical mean-field theory (DMFT) [22,23]. This approach has already been successfully employed to compute the electronic structure and optical absorption edge in the rare-earth fluorosulfide pigments LnSF (with Ln = rare-earth) [16]. We demonstrate that the same computational approach can be applied to $YIn_{1-x}Mn_xO_3$, where it gives valuable insight into the mechanisms that are responsible for the blue coloration of the pigment. We further model the diffuse reflectance of the milled pigment using the effective medium description by Kubelka and Munk [24,25], and compare our results to available experimental data.

II. COMPUTATIONAL APPROACH

We start from the experimental $P6_3cm$ crystal structure of $YInO_3$. We double the unit cell in $\hat{\boldsymbol{c}}$ direction and replace one of the 12 In atoms with Mn (note that all In in the supercell have the same symmetry, Wyckoff site c), which yields a Mn concentration of $x \approx 8\%$ in the supercell. For numerical feasibility, we perform all calculations with this supercell, thus neglecting effects of disorder. The a and c lattice parameters, which show a clear linear dependence with Mn concentration x, are extracted from experimental measurements of Ref. [14]. For $x \approx 8\%$, this yields $a = 6.2620$ Å and $c = 12.1788$ Å. We relax all internal coordinates within DFT, employing a full-potential linear-augmented plane-wave basis set, as implemented in the WIEN2k [26,27] program package. In the structural relaxations, a multisecant approach [27] with a $\mathbf{k}$ grid of 100 $\mathbf{k}$ points in the reducible Brillouin zone was used and atomic positions were relaxed until forces were less than 1 mRy/bohr. We performed relaxations, both, within LDA and LSDA+U. We found the LSDA+U-relaxed structure to be virtually unaffected by changes of U within a window of 3−8 eV. Also the type of the imposed (artificial) magnetic order (ferro- or antiferromagnetic) had no influence on the result. The LDA-relaxed structure, instead, displayed a slightly different local crystalline environment around the Mn^{3+} ions, which compared better to experiment [14] (see Results and the Appendices). We therefore focus on the LDA-relaxed structure, but compare the optical conductivity of both relaxations to highlight the influence of the local crystal structure onto the color.

To compute the electronic structure and optical conductivity of paramagnetic $YIn_{1-x}Mn_xO_3$ (with $x \approx 8\%$), we employ the recently developed mBJ@DFT+DMFT approach, for details of the method see Ref. [18]. It basically consists of three steps:

(1) We start by performing a charge-self-consistent DFT+DMFT calculation [26,28–30], in which we treat local correlations in the Mn $3d$ shell with the quasi-atomic Hubbard-I [31] DMFT solver. To this end, we construct projective Wannier functions [28,30] representing the correlated Mn $3d$ states from all Kohn-Sham eigenstates enclosed by the energy window $[-9, 10]$ eV around the Fermi level. In the spirit of previous DMFT calculations for other transition-metal oxides [32,33], we mimic a d-only (downfolded) setting by limiting the hybridization function to an energy window of $[-1, 3]$ eV, accounting for 92% of the Mn spectral weight from the large energy window. We use the electronic structure code WIEN2k [26] for DFT and the TRIQS [34] and TRIQS/DFTTools [30] packages for DMFT.

(2) After converging the charge-self-consistent DFT+DMFT calculations, we run an additional DFT cycle employing the Tran-Blaha modified Becke-Johnson (mBJ) potential [20,21], as implemented in WIEN2k [26]. Such a perturbative use of the mBJ potential was shown to yield reliable values for semiconducting band gaps [35]. For the problem at hand, we demonstrate (see Appendix A) that a perturbative use of the mBJ potential yields a value of 3.71 eV for the band gap in pure $YInO_3$, which is in good agreement with the experimental value of around 3.8 eV, estimated from the diffuse reflectance measured in Ref. [2].

(3) After the perturbative mBJ step, we finally recalculate the electronic structure of $YIn_{1-x}Mn_xO_3$ by performing a DMFT cycle using the Hubbard-I approximation for the mBJ-corrected Kohn-Sham bands.

Our calculations do not break spin-symmetry (paramagnetic) and the Mn $3d$ quantum impurity problem contains all five Mn $3d$ orbitals. The fully rotationally-invariant local Coulomb interaction on the Mn $3d$ shell was parametrized by $U = 2.5$ eV and $J = 0.8$ eV. Previous studies [2] suggested

the Mn-multiplet structure to be a crucial ingredient for the material's color. The Hubbard U parameter was therefore deliberately chosen to be of a magnitude comparable to visible light. Ideally, the interactions should be computed from first principles in the future. We further employed the fully-localized-limit double-counting correction in the atomic limit [36], i.e., $E_{DC} = U(N - 0.5) - J(0.5N - 0.5)$ with the Mn^{3+} atomic occupancy $N = 4$. All calculations were carried out at a temperature of 290 K.

As a result of the mBJ@DFT+DMFT calculations, we obtain the many-body spectral function $A_{\mathbf{k}}(\omega)$ encoding the excitation energies of an electron addition/removal into the many-body ground state. $A_{\mathbf{k}}(\omega)$ is a crucial ingredient for determining the absorption properties of a crystalline bulk material. By using linear response theory, and neglecting vertex corrections, the real part of the frequency-dependent optical conductivity reads [37,38]

$$\sigma_{\alpha\alpha}(\Omega) = \frac{2\pi e^2\hbar}{V}\sum_k \int d\omega\, \frac{f(\omega-\Omega/2) - f(\omega+\Omega/2)}{\Omega} \times \mathrm{Tr}\{\mathbf{A}_{\mathbf{k}}(\omega-\Omega/2)\mathbf{v}_{\mathbf{k},\alpha}\mathbf{A}_{\mathbf{k}}(\omega+\Omega/2)\mathbf{v}_{\mathbf{k},\alpha}\}, \quad (1)$$

where V is the unit-cell volume, Ω the frequency of the incident light and $f(\omega \pm \Omega/2)$ Fermi functions which ensure that transitions take place only between occupied and empty states. As usual, we limit the calculation to direct optical transitions, without any momentum transfer [37]. $\mathbf{v}_{k,\alpha}$ are matrix elements of the momentum operator in the Cartesian directions $\alpha = x, y,$ or z [39], and $\mathbf{A}_{\mathbf{k}}(\omega)$ are the $\mathbf{k}$-resolved spectral-function matrices in orbital space. The complex conductivity $\tilde{\sigma}(\omega)$ can be constructed from $\sigma(\omega)$ using a Kramers-Kronig transform.

To study the influence of individual orbitals and matrix elements in the optical response, we compare $\sigma(\omega)$ to the partial joint density of states

$$D_l(\Omega) \propto \int d\omega\, \frac{f(\omega-\Omega/2) - f(\omega+\Omega/2)}{\Omega} \times A_l(\omega-\Omega/2)A_l(\omega+\Omega/2) \quad (2)$$

where $A_l(\omega)$ is the local spectral function traced over the orbital character l. When computing optical properties, we use a refined mesh of 1000 $\mathbf{k}$ points in the reducible Brillouin zone, a frequency spacing of 1 meV and an additional broadening of excitations $\delta = 0.8$ meV.

Since pigments are used in powdered form or lacquers, i.e., as small particles within a transparent glaze, in principle a complicated multiple-scattering problem needs to be solved to obtain the diffuse reflectance R. A simple and commonly used shortcut is the effective medium description by Kubelka and Munk (KM) [24,25], which models the propagation of light through a homogeneous layer with a pigment concentration $c_{\%}$, that absorbs light with an amplitude $c_{\%}K(\omega)$ and backscatters it with rate $\beta(\omega)$. Here, $K(\omega)$ is the macroscopic absorption coefficient of the pigment's crystalline bulk, linked to the complex conductivity $\tilde{\sigma}$ via $K(\omega) = \omega/c\,\Im(\sqrt{1 + \frac{4\pi i}{\omega}\tilde{\sigma}(\omega)})$ with c the speed of light. The parameter $\beta(\omega)$—an inverse scattering length—contains information on the imperfect microscopic structure of the sample and is often treated as phenomenological and static ($\beta(\omega) \equiv \beta$) [15]. In the KM model, the diffuse reflectance of a semi-infinite pigment layer is given by

$$R_\infty(\omega) = \alpha - \sqrt{\alpha^2 - 1}, \quad \text{with} \quad \alpha = 1 + \frac{2c_{\%}K(\omega)}{\beta}. \quad (3)$$

Supplementing the simulated diffuse reflectance with the spectral distribution of a light source—we use the CIE standard illuminant D65 [40] corresponding to daylight on Earth—and the empirical sensitivities for the color perception of the human eye [41], we compute the coordinates in the sRGB color space [42], predicting the color of $YIn_{1-x}Mn_xO_3$.

TABLE I. M-O bond lengths ℓ and the absolute difference in axial distances Δ_{axial} of pure $YInO_3$ and $YIn_{1-x}Mn_xO_3$. Theoretical bond lengths were obtained by LDA. Experimental data are reproduced from Table II of Ref. [14]. Note that our calculation for $YIn_{1-x}Mn_xO_3$ were performed for x = 8.33%, while the experiment [14] was carried out for x = 5%.

ℓ [Å]	$YInO_3$		$YIn_{1-x}Mn_xO_3$	
Bond	Exp.	LDA	Exp.	LDA
Axial 1	2.089	2.088	1.879	1.891
Axial 2	2.093	2.111	2.087	2.045
Δ_{axial}	0.004	0.023	0.208	0.154
Equatorial 1	2.097	2.130	1.976	1.862
Equatorial 2	2.127	2.122	1.976	1.862
Equatorial 3	2.127	2.122	2.087	1.885

III. RESULTS

A. Crystal structure

Our structural relaxations confirm the previously observed trend [2,12–14] of decreasing axial M-O bond distances in the trigonal bipyramids (TBPs) of YMO_3, when In^{3+} ions are replaced with the smaller Mn^{3+}. The equatorial bond lengths are less affected by the Mn substitution. Table I further shows an axial distortion of the TBPs for small Mn concentrations, $x = 8\%$, expanding one of the axial Mn-O bonds by ∼10%. These asymmetric bond lengths have indeed been observed in XANES and EXAFS experiments [14] and were claimed to be important for the blue coloration of $YIn_{1-x}Mn_xO_3$ as they change the local crystalline environment of the Mn^{3+} ions. In our calculations, clearly asymmetric axial bond distances are observed only in the LDA-relaxed structure, see Table I. The effect is much less pronounced for relaxations with LSDA+U (see Table II in Appendix B). For the electronic structure and optical calculations, we therefore proceed with the LDA-relaxed structure. For comparison, we also perform computations of the optical conductivity with symmetric axial Mn-O bond distances (LSDA+U relaxed structure). This way, we can analyze how the optical response and color of the pigment are affected by different local crystalline environments around the Mn^{3+} ions, which have been argued [14] to be present in the disordered solid-solution.

TABLE II. M-O bond lengths ℓ of $YIn_{1-x}Mn_xO_3$, for various Mn concentrations x (for $x = 0$, In-O bonds are reported; for all other x Mn-O ones). Shown are the results of the structural relaxations within LDA and LSDA+U ($U = 5$ eV, $J = 0.5$ eV), as well as experimental data taken from Ref. [14].

	$x = 0$		$x = 5\%$	$x = 8.3\%$		$x = 1$		
Bond	ℓ [Å]Exp.	ℓ [Å] LDA	ℓ [Å]Exp.	ℓ [Å] LDA	ℓ [Å] LSDA+U	ℓ [Å]Exp.	ℓ [Å] LDA	ℓ [Å] LSDA+U
Axial 1	2.089	2.088	1.879	1.891	1.910	1.848	1.856	1.867
Axial 2	2.093	2.111	2.087	2.045	1.916	1.882	1.875	1.869
Equatorial 1	2.097	2.130	1.976	1.862	2.035	1.966	2.163	2.066
Equatorial 2	2.127	2.122	1.976	1.862	2.035	2.118	2.002	2.058
Equatorial 3	2.127	2.122	2.087	1.885	2.035	2.118	2.002	2.058

B. Electronic structure and optical response

We begin with the electronic structure of crystalline bulk $YIn_{1-x}Mn_xO_3$ (with $x = 8.33\%$). Figure 2(a) shows the **k**-resolved spectral function $A_{\mathbf{k}}(\omega)$, as obtained from mBJ@DFT+DMFT. The chosen **k** path through the Brillouin zone is specified in Fig. 8 and the **k**-integrated spectral function $A(\omega)$ is depicted in Fig. 2(b). The valence band below –2.8 eV (energies measured from Fermi level), is mainly formed by the filled O 2p states. The conduction band starts at around 1.2 eV with some dispersive bands of mainly In 5s character, before Y 4d bands appear above 4.5 eV. The simulated O-2p – In-5s band gap in $YIn_{0.92}Mn_{0.08}O_3$ thus amounts to 4 eV, which is close to the predicted and experimental value for pure $YInO_3$ (see Appendix A). At a concentration of 8%, the Mn atoms are fairly isolated. Accordingly, their 3d states form sharp peaks in the local spectral function, corresponding to only weakly-dispersive quasi-atomic multiplets. The most prominent part of the lower Hubbard band, i.e., the occupied Mn 3d states directly below the Fermi energy and at –1.8 eV, are located within the O-2p – In-5s band gap. The multiplet peaks of the Mn-3d upper Hubbard band lie within the dispersive conduction bands, with sizable features visible in a window of 2–6 eV.

The Mn 3d states play a crucial role in the optical response of $YIn_{0.92}Mn_{0.08}O_3$, as can be seen in Fig. 2(c), which depicts the simulated optical conductivity $\sigma(\omega) \equiv \sum_\alpha \sigma_{\alpha\alpha}(\omega)/3$ averaged over polarizations α [see Eq. (1)] as well as the partial joint density of states (JDOS; see Sec. II) of the Mn 3d states $D_{3d}(\omega)$. One can clearly see that $\sigma(\omega)$ exhibits two dominant peaks in the energy range from 1.2–4 eV. Such a two-peak structure is crucial for any blue coloration since it allows for absorption on the low- as well as high-energy side of the optical spectrum, while reflecting the blue components (2.5–2.8 eV). The shallow onset of the first absorption peak at around 1.2 eV stems from optical transitions from the highest occupied Mn 3d states [red peak in $A(\omega)$ just below the Fermi energy] to the bottom of the dispersive conduction band. The principle weight of the absorption peak at around 2–2.5 eV, instead, can be traced to $d - d$ transitions. Indeed, a comparison with the partial JDOS $D_{3d}(\omega)$ suggests optical transitions

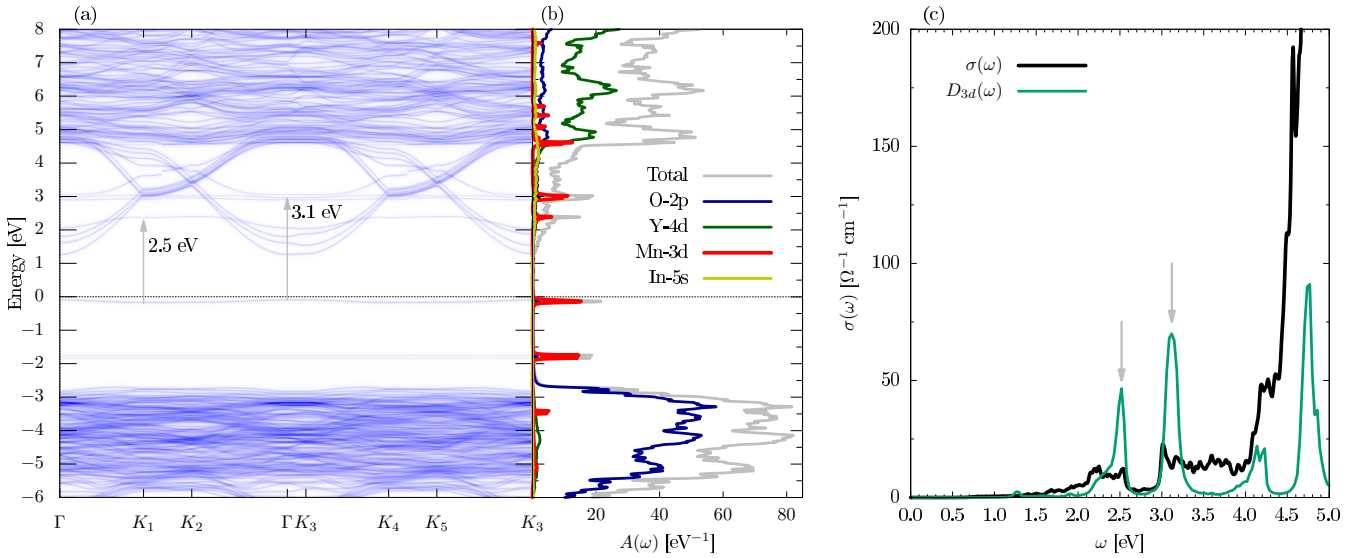

FIG. 2. Electronic structure and optical conductivity of $YIn_{0.92}Mn_{0.08}O_3$ (a) **k**-resolved and (b) **k**-summed spectral function obtained from mBJ@DFT+DMFT. The valence band (below –2.8 eV) is formed by the O 2p (blue) states. The conduction band involves some dispersive bands (starting a 1.2 eV) with mainly In 5s (yellow) character and Y 4d (green) states above 4.5 eV. The Mn 3d states are split into multiplets by the on-site Coulomb interaction. The occupied Mn 3d orbitals form impurity states within the band gap. In (c) we show the computed (polarization-averaged) optical conductivity $\sigma(\omega)$ (black). The two-peak structure between 1.2–4 eV, which is crucial for the blue color, arises mainly from Mn $d - d$ optical transitions, as can be seen by comparing to the partial joint density of states $D_{3d}(\omega)$ (green).

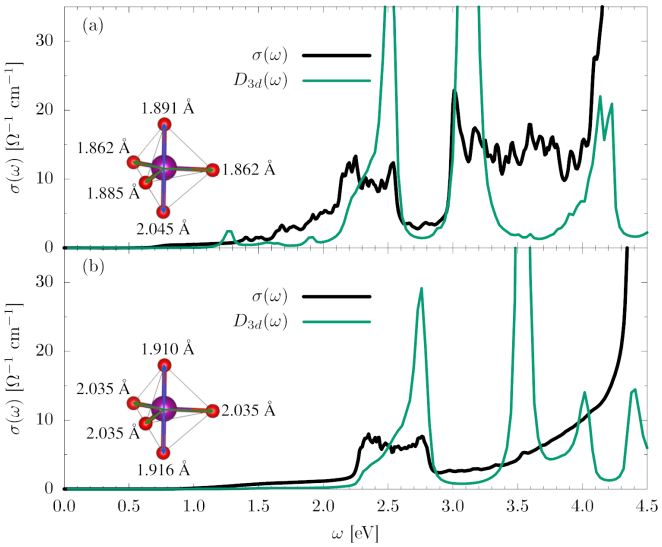

FIG. 3. Effect of asymmetric axial Mn-O bonds. (a) The optical conductivity (black) of $YIn_{0.92}Mn_{0.08}O_3$ with asymmetric axial Mn-O bond lengths shows a characteristic two-peak structure between 1.2–4 eV arising mainly from Mn $d-d$ optical transitions [detail of Fig. 2(c)]. (b) A simulation with symmetric axial Mn-O bonds shows that the second peak centered around 3.5 eV in the partial Mn $3d$ JDOS (green) disappears in the optical conductivity (black) due to the influence of optical transition matrix elements. Input electronic structures were computed with mBJ@DFT+DMFT.

from the highest occupied to the lowest unoccupied Mn $3d$ states to be active. In an atom, such $d-d$ optical transitions would be forbidden by the dipole selection rules. In a solid, the crystal field, hybridization with ligands, as well as nonlocal transitions can relax the optical selection rules so that $d-d$ processes become possible. The onset of the second prominent absorption peak at 3 eV is in fact also dominated by optical $d-d$ transitions. In this case, the relevant transitions happen between the occupied Mn $3d$ states just below the Fermi level and the unoccupied Mn $3d$ states around 3 eV. This second, broad peak in $\sigma(\omega)$ then continues until around 4 eV with transitions from Mn $3d$ into the conduction band. At around 4 eV, optical transitions from the O $2p$ valence band to the conduction band set in, leading to a rapid increase of the optical conductivity.

In order to identify the effect of the axially distorted TBP on the optical response of $YIn_{0.92}Mn_{0.08}O_3$, we perform calculations with symmetric axial Mn-O bonds for comparison, using the crystal structure relaxed within LSDA+U. The latter did not show any asymmetry in the axial bonds (see Appendix A, Table II). Figure 3 represents a direct comparison between the optical conductivity $\sigma(\omega)$ of $YIn_{0.92}Mn_{0.08}O_3$ calculated with (a) asymmetric axial Mn-O bonds as in Fig. 2 and (b) assuming symmetric axial Mn-O bond lengths in the TBP. While Fig. 3(a) shows the characteristic two-peak structure of $\sigma(\omega)$ already discussed in Fig. 2(c), Fig. 3(b) looks strikingly different. The partial Mn $3d$ JDOS, $D_{3d}(\omega)$, still displays two peaks centered at 2.7 and 3.5 eV, respectively. Compared to Fig. 3(a), these peaks are located at slightly different energies due to the change in the local crystalline environment of the Mn^{3+} ions. More importantly, the main difference between $\sigma(\omega)$ in Figs. 3(a) and 3(b) is the absence of the second peak at 3.5 eV for symmetric TBP. Since the principle difference between the JDOS $D_{3d}(\omega)$ and the optical conductivity $\sigma(\omega)$ stems from the transition-matrix elements $v_{\alpha\mathbf{k}}$ [see Eq. (1)], we assign the suppression of the peak at 3.5 eV to the latter. Intuitively, one can indeed suspect the axial distortion—introduced by the asymmetric TBP—to further relax the optical dipole selection rules. This conjecture is supported by inspecting the momentum-resolved spectra [compare Fig. 2(a) with Fig. 7 of Appendix C]: In the case of the undistorted TBP—with symmetric axial Mn-O bonds—the Mn-states are visibly less dispersive and hence closer to the atomic limit, for which the dipole selection rule applies. The correspondence between dispersion and transition-matrix elements is explicit in the Peierls approximation, in which inter-unitcell transitions are weighted with $v_{\alpha\mathbf{k}} = \hbar^{-1} d/dk_\alpha H_0(\mathbf{k})$, where H_0 is the noninteracting Hamiltonian [38].

In the experimental investigations of Ref. [14] it had already been suspected that the axial distortion of the TBP is important for the blue coloration of $YIn_{1-x}Mn_xO_3$. Our optical simulations fortify this understanding. The asymmetric Mn-coordination causes optical transitions that are possible energetically to also become dipole allowed. This circumvention of the atomic selection rule is a requirement for the two-peak structure in the visible absorption and, hence, for the blue color.

C. Diffuse reflectance and color of the pigment

We continue by computing the diffuse reflectance $R(\lambda)$ as a function of wavelength $\lambda = 2\pi c/\omega$, using Eq. (3) and the optical conductivity from mBJ@DFT+DMFT. In Fig. 4 we compare the theoretical diffuse reflectance of

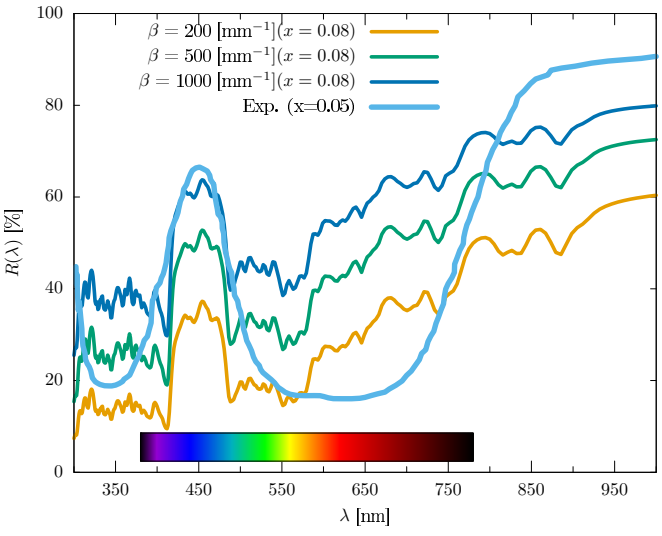

FIG. 4. Computed diffuse reflectance $R(\lambda)$ compared to experiment. The theoretical curves for various values of the scattering parameter $\beta = 200, 500, 1000\,\mathrm{mm}^{-1}$ (in orange, green, and dark blue, respectively) all show a prominent reflectance peak in the blue region, which agrees well with experiment (light blue, data from Ref. [43], for $x = 5\,\%$). In the red region of the spectrum, the computed diffuse reflectance is too high compared to experiment.

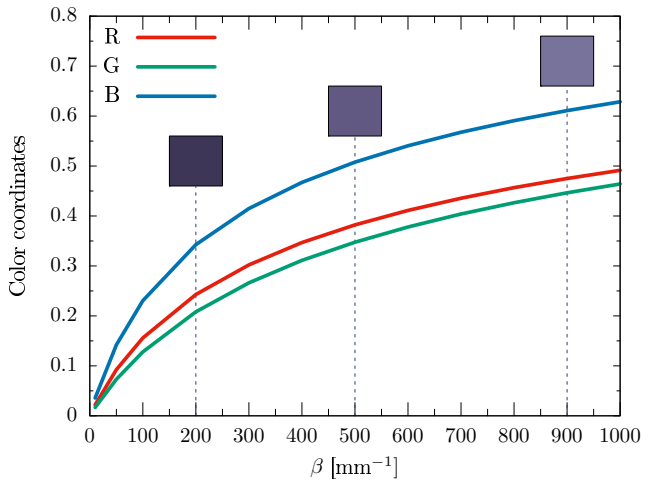

FIG. 5. Simulated color coordinates of $YIn_{0.92}Mn_{0.08}O_3$, $R, G, B \in [0, 1]$, calculated as a function of the scattering parameter β for a nondiluted sample ($c_{\%} = 1$), and apparent color (squares).

$YIn_{0.92}Mn_{0.08}O_3$, for several values of the scattering parameter β, to the experiment of Ref. [43]. We notice that the theoretical curves all display a pronounced reflectance peak in the blue region, which nicely matches with experiment. This reflectance peak arises from the discussed two-peak structure in the optical conductivity and is responsible for the blue color. With increasing β also $R(\lambda)$ increases, as more incoming light is backscattered, while the overall shape of $R(\lambda)$ does not change significantly. On the low-energy side of the visible spectrum, the agreement between theory and experiment is less convincing. Our simulations show a non-negligible reflectance especially in the red region, which can be traced back to the weak onset of optical transitions in the 1.2–2.2 eV energy range.

Finally, we compute the apparent color of the pigment, assuming a sample of concentration $c_{\%} = 1$. Figure 5 shows the resulting $(R, G, B) \in [0, 1]^3$ color coordinates as a function of β with (0,0,0) and (1,1,1) being black and white, respectively. Since the reflectance depends on β, also the color coordinates (R, G, B) do. Our results show that the blue B component dominates over the entire β range, as expected. Sizable admixtures from the R and G components result in an overall steal-blue color in the simulation, while experimental probes exhibit a deeper blue coloration.

IV. CONCLUSIONS

We have presented an attempt to compute the optical response and color of the blue pigment $YIn_{1-x}Mn_xO_3$ from first principles. We employed the recently developed mBJ@DFT+DMFT approach and confirmed—after its application to the rare-earth fluorosulfide pigments [16]—that this approach represents a useful computational tool for addressing the electronic structure of correlated pigment materials. In $YIn_{1-x}Mn_xO_3$, and pure $YInO_3$, the semilocal mBJ exchange potential successfully corrects the band gap between O $2p$ and In $5s$ states, which is significantly underestimated in LDA. The DMFT, instead, is able to treat the strong on-site Coulomb interaction in the Mn $3d$ shell.

We found that the optical response of $YIn_{0.92}Mn_{0.08}O_3$ close to the blue part of the spectrum is strongly influenced by the quasi-atomic Mn $3d$ states: Optical d-d transitions yield a well-defined two-peak structure in the absorption, necessary for the blue coloration. The splitting of the Mn $3d$ states is driven by multiplet effects and the local crystalline environment around the Mn^{3+} ions. An important finding of our work is that asymmetric axial distortions of the trigonal bipyramid surrounding the manganese impurities are a prerequisite for the blue color: They weaken the atomic dipole selection rule, so that $d - d$ absorption becomes permissible. Our work thus establishes a direct link between the asymmetry of the Mn^{3+} coordination polyhedron and the blue coloration of $YIn_{0.92}Mn_{0.08}O_3$. The weak absorption in the red-yellow region, due to optical transitions from Mn $3d$ to the dispersive bottom of the In $5s$ dominated conduction band, makes the pigment appear steal blue in our calculations. Future investigations need to address the effect of Mn disorder, as well as trends for varying Mn concentration.

ACKNOWLEDGMENTS

This work is based on the results of the Master thesis [44] of V.R. at TU Wien. We thank L. V. Pourovskii, J. Boust, S. Biermann, and A. Smolyanyuk for helpful discussions. We further acknowledge financial support by Schrödinger Fellowship Grant No. J-4267 of the Austrian Science Fund (FWF). Calculations were performed on the Vienna Scientific Cluster VSC4.

APPENDIX A: ELECTRONIC STRUCTURE OF $YInO_3$

In Fig. 6 we show the density of states (DOS) of pure $YInO_3$ computed within (a) LDA and (b) mBJ@LDA. The latter refers to the perturbative use [35] of the mBJ potential [20] on top of a converged LDA calculation. In LDA, the band gap between the O $2p$ dominated valence band and the bottom of the conduction band of mainly In $5s$ character is only

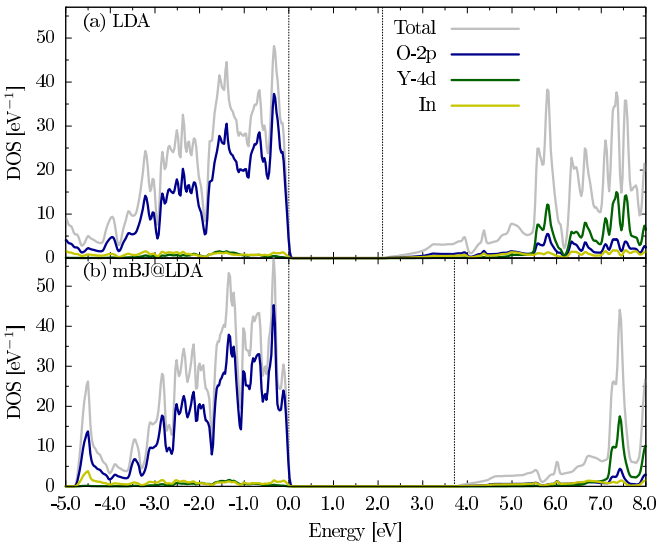

FIG. 6. Density of states of $YInO_3$ calculated with (a) LDA and (b) mBJ@LDA. The dashed-vertical lines indicate the band gap.

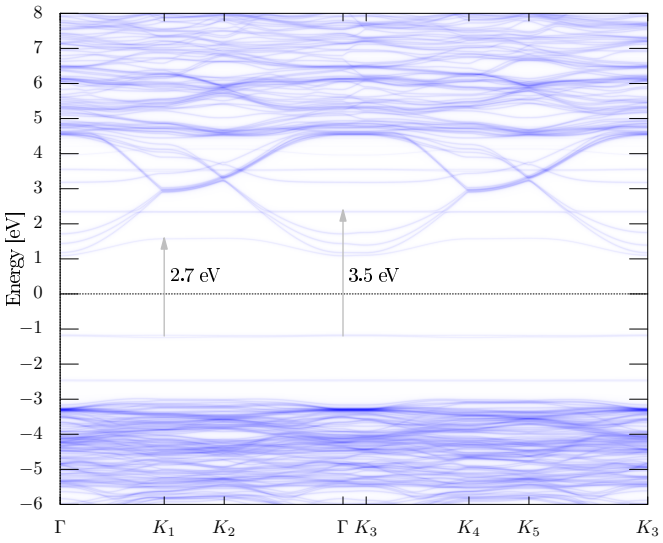

FIG. 7. **k**-resolved spectral function of $YIn_{0.92}Mn_{0.08}O_3$ with symmetric axial Mn-O bonds (bond lengths from LSDA+U relaxation, see Table II). The Mn 3d states are flatter and more atomic-like than in Fig. 2(a).

2.1 eV wide and thus significantly underestimated compared to its experimental value of approximately 3.8 eV (which can be inferred from the diffuse reflectance of $YInO_3$ measured in Ref. [2]). The mBJ potential, which effectively mimics nonlocal exchange, corrects the band gap to 3.71 eV, which is in good agreement with experiment. Since such a perturbative use of the mBJ potential gives good results for pure $YInO_3$, we conclude that it is also well suited for $YIn_{1-x}Mn_xO_3$, with small Mn concentrations x.

APPENDIX B: SUMMARY OF COMPUTED BOND LENGTHS

In Table II we summarize the results of our structural relaxations performed within LDA and LSDA+U. Reported are computed axial and equatorial M-O bond lengths ℓ for pure $YInO_3$ ($x = 0$), $YIn_{1-x}Mn_xO_3$ ($x = 0.083$), and $YMnO_3$ ($x = 1$). For comparison, we also reproduce experimental values for $x = 0, 0.05, 1$ extracted from Ref. [14]. For small Mn concentrations $x = 0.05, 0.083$, experiment and LDA relaxations show a clear axial asymmetry, in that one of the axial Mn-O bonds in the TBPs expands by ∼10%. Equatorial bond lengths slightly differ from experiment. Remarkably, the LSDA+U relaxation for $x = 0.083$ does not show any axial distortion of the TBPs. This difference might originate from the artificial magnetic order assumed in LSDA+U. However, we cannot exclude that our simulations converged to a local energy minimum often encountered in LSDA+U calculations.

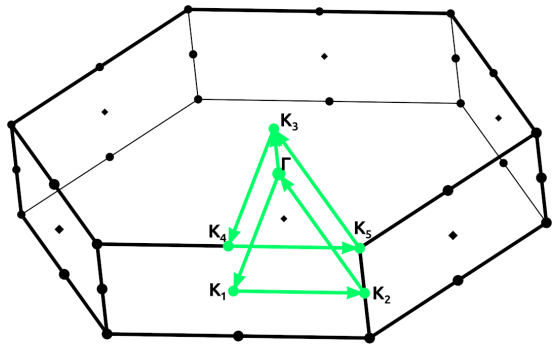

FIG. 8. Primitive Brillouin zone (BZ) of $YIn_{0.92}Mn_{0.08}O_3$ plotted with `XCrySDen` [45]. The **k** path through the BZ ($\Gamma - K_1 - K_2 - \Gamma - K_3 - K_4 - K_5 - K_3$) is marked by green arrows.

APPENDIX C: SPECTRAL FUNCTION WITH SYMMETRIC AXIAL MN-O BONDS

Figure 7 shows the **k**-resolved mBJ@DFT+DMFT spectral function of $YIn_{0.92}Mn_{0.08}O_3$ assuming symmetric axial Mn-O bonds in the TBPs (structure relaxed within LSDA+U, bond lengths as specified in Table II). The Mn 3d bands are flatter and more atomic-like compared to Fig. 2, completely suppressing the $d - d$ transitions in the optical conductivity at 3.5 eV, see Fig. 3(b).

The **k** path through the hexagonal Brillouin zone (BZ) of $YIn_{0.92}Mn_{0.08}O_3$, employed in Fig. 7 and Fig. 2(a), is shown in Fig. 8.

[1] N. Eastaugh, V. Walsh, T. Chaplin, and R. Siddall, *Pigment Compendium: A Dictionary and Optical Microscopy of Historical Pigments* (Routledge, New York, 2008)

[2] A. E. Smith, H. Mizoguchi, K. Delaney, N. A. Spaldin, A. W. Sleight, and M. A. Subramanian, J. Am. Chem. Soc. **131**, 17084 (2009).

[3] M. A. Subramanian and J. Li, Nat. Rev. Mater. (2022).

[4] M. Ocaña, J. Espinós, and J. Carda, Dyes Pigm. **91**, 501 (2011).

[5] Y. Gomes, J. Li, K. Silva, A. Santiago, M. Bomio, C. Paskocimas, M. Subramanian, and F. Motta, Ceram. Int. **44**, 11932 (2018).

[6] Y. F. Gomes, *Síntese e caracterizao do pigmento azul YInMnO pelo método de polimerizao de complexos (MPC)*,Ph.D. thesis, Universidade Federal do Rio Grande do Norte, Brazil, 2018.

[7] YInMn blue, 200 years in the making, https://www.shepherdcolor.com/yinmn-blue/ (2017), accessed: 2022-06-30.

[8] M. A. Subramanian, A. W. Sleight, and A. E. Smith, Materials with trigonal bipyramidal coordination and methods of making the same, (2012), US Patent 8282728 B2.

[9] K. Momma and F. Izumi, J. Appl. Cryst. **44**, 1272 (2011).

[10] R. D. Shannon, Inorg. Chem. **6**, 1474 (1967).

[11] C. Pistorius and G. Kruger, J. Inorg. Nucl. Chem. **38**, 1471 (1976).

[12] M. El Amrani, V. Ta Phuoc, M. Ammar, M. Zaghrioui, and F. Gervais, Solid State Sci. **14**, 1315 (2012).

[13] J. Li, A. W. Sleight, and M. A. Subramanian, Chem. Mater. **28**, 6050 (2016).

[14] S. Mukherjee, H. Ganegoda, A. Kumar, S. Pal, C. U. Segre, and D. D. Sarma, Inorg. Chem. **57**, 9012 (2018).

[15] J. M. Tomczak, L. V. Pourovskii, L. Vaugier, A. Georges, and S. Biermann, Proc. Natl. Acad. Sci. USA **110**, 904 (2013).
[16] A. Galler, J. Boust, A. Demourgues, S. Biermann, and L. V. Pourovskii, Phys. Rev. B **103**, L241105 (2021).
[17] S. Acharya, C. Weber, D. Pashov, M. van Schilfgaarde, A. I. Lichtenstein, and M. I. Katsnelson, arXiv:2204.11081.
[18] J. Boust, A. Galler, S. Biermann, and L. V. Pourovskii, Phys. Rev. B **105**, 085133 (2022).
[19] A. Galler and L. V. Pourovskii, New J. Phys. **24**, 043039 (2022).
[20] F. Tran and P. Blaha, Phys. Rev. Lett. **102**, 226401 (2009).
[21] D. Koller, F. Tran, and P. Blaha, Phys. Rev. B **83**, 195134 (2011).
[22] W. Metzner and D. Vollhardt, Phys. Rev. Lett. **62**, 324 (1989).
[23] A. Georges and G. Kotliar, Phys. Rev. B **45**, 6479 (1992).
[24] P. Kubelka and F. Munk, Z. Tech. Phys. **12**, 593 (1931).
[25] P. Kubelka, J. Opt. Soc. Am. **38**, 448 (1948).
[26] P. Blaha, K. Schwarz, G. Madsen, D. Kvasnicka, J. Luitz, R. Laskowski, F. Tran, and L. D. Marks, *WIEN2k, An augmented Plane Wave + Local Orbitals Program for Calculating Crystal Properties* (Karlheinz Schwarz, Techn. Universität Wien, Austria, 2018).
[27] P. Blaha, K. Schwarz, F. Tran, R. Laskowski, G. K. H. Madsen, and L. D. Marks, J. Chem. Phys. **152**, 074101 (2020).
[28] M. Aichhorn, L. Pourovskii, V. Vildosola, M. Ferrero, O. Parcollet, T. Miyake, A. Georges, and S. Biermann, Phys. Rev. B **80**, 085101 (2009).
[29] M. Aichhorn, L. Pourovskii, and A. Georges, Phys. Rev. B **84**, 054529 (2011).
[30] M. Aichhorn, L. Pourovskii, P. Seth, V. Vildosola, M. Zingl, O. E. Peil, X. Deng, J. Mravlje, G. J. Kraberger, C. Martins *et al.*, Comput. Phys. Commun. **204**, 200 (2016).
[31] J. Hubbard, Proc. Roy. Soc. (London) **A 276**, 238 (1963).
[32] L. V. Pourovskii, D. F. Mosca, and C. Franchini, Phys. Rev. Lett. **127**, 237201 (2021).
[33] H. Banerjee and M. Aichhorn, Phys. Rev. B **101**, 241112(R) (2020).
[34] O. Parcollet, M. Ferrero, T. Ayral, H. Hafermann, I. Krivenko, L. Messio, and P. Seth, Comput. Phys. Commun. **196**, 398 (2015).
[35] H. Jiang, J. Chem. Phys. **138**, 134115 (2013).
[36] L. V. Pourovskii, B. Amadon, S. Biermann, and A. Georges, Phys. Rev. B **76**, 235101 (2007).
[37] M. Dresselhaus, *Optical Properties of Solids* (MIT Lecture Notes, 2001).
[38] J. M. Tomczak and S. Biermann, Phys. Rev. B **80**, 085117 (2009).
[39] C. Ambrosch-Draxl and J. O. Sofo, Comput. Phys. Commun. **175**, 1 (2006).
[40] Joint ISO/CIE Standard S005/E-1998, *CIE Standard Illuminants for Colorimetry* (ISO/CIE, 1999).
[41] W. D. Wright, Opt. Soc. **30**, 141 (1929).
[42] M. Anderson, R. Motta, S. Chandrasekar, and M. Stokes, in *Proc. IS&T 4th Color and Imaging Conference* (Society for Imaging Science and Technology, 1996), pp. 238–245.
[43] J. Li, S. Lorger, J. K. Stalick, A. W. Sleight, and M. A. Subramanian, Inorg. Chem. **55**, 9798 (2016).
[44] V. Ransmayr, *A DFT+DMFT study of the electronic structure and optical properties of the blue pigment material* $YIn_{1-x}Mn_xO_3$, Master's thesis, Techn. Universität Wien, Vienna, 2022, https://doi.org/10.34726/hss.2022.102630.
[45] A. Kokalj, J. Mol. Graphics Modell. **17**, 176 (1999), code available at http://www.xcrysden.org/.